Continuous thermogravimetric analysis during the cyclic oxidation of Ni–22Al–15Pt + 1 wt.% Hf at 1200 °C

R. Kartono,[a] D. Monceau[b,*] and D.J. Young[a]

[a] *School of Materials Science and Engineering, UNSW, Sydney, Australia*
[b] *CIRIMAT Laboratory, University of Toulouse, ENSIACET, 31077 Toulouse, France*

Cyclic thermogravimetric analysis (CTGA) provided a quantitative assessment of cyclic oxidation kinetics for a Ni–22Al–15Pt + 1 wt.% Hf alloy. This alloy showed a very low extent of oxide spallation and a slow oxidation rate. The adherent oxide thickness calculated from observed weight changes (due to both oxidation and scale loss) was found to be very similar to the directly measured scale thickness. It is concluded that a previously developed description of cyclic oxidation thermogravimetry is applicable, and that the alloy exhibits excellent performance.

Keywords: Thermogravimetric analysis; Nickel alloys; Oxidation; CTGA

Cyclic oxidation gravimetric data is usually obtained from discontinuous experiments [1,2] in which samples are periodically removed from the reaction furnace to be weighed, and then replaced. In order to obtain reproducible cooling and heating rates, as well as precisely defined dwell times at high and low temperature, an automated cyclic oxidation test is preferred [1]. Two different methods are commonly used for obtaining kinetics from discontinuous cyclic oxidation experiments:

1. Weighing the sample periodically and replacing it in the furnace [1,2].
2. The same, but the sample is contained in an open or closed crucible to capture spalled oxide [3].

In case 1, the net sample mass change (NMC) is the only data that can be obtained. However, in case 2, both NMC and gross mass gain (GMG, i.e. including spalled oxide inside the crucible) can be measured. In case 1, it is impossible to determine individually the total oxygen uptake and the mass loss due to oxide spallation [1,4]. In case 2, this difficulty is in principle removed, but experimental problems arise: it is impossible to obtain rapid heating and cooling, because of the crucible thermal mass; it is difficult to ensure that specimens experience a constant gas flow, a critical issue in mixed gases; variations in crucible mass may decrease the measurement precision; some spalled oxide may escape from open containers. Both experiments present practical difficulties in specimen handling. Exposure to the laboratory atmosphere during handling may affect the results if ambient humidity changes oxide spallation behaviour [5].

In general, there are three different methods to estimate NMC and GMG data for evaluating cyclic oxidation performance:

1. Crucible tests with the various practical problems described above [4].
2. The application of spallation modelling to discontinuous measurements [6–8] in order to obtain the spallation probability, P, and the parabolic rate constant, k_p.
3. Cyclic TGA [9] to measure NMC and GMG [10], with the advantage of spallation detection in real time.

The last technique has been used, for example, to characterize cyclic oxidation kinetics of a nickel-based superalloy with and without a coating [11]. Its use is described here in the evaluation of a cast Ni–22Al–15Pt (at.%) alloy modified by the addition of 1 wt.% Hf. This alloy has been found [12] to have excellent high temperature corrosion resistance and [13] to perform very well at 1200 °C in conventional cyclic oxidation tests.

The experiment was performed in flowing synthetic dry air at 1200 °C, using a SETARAM TAG 24S thermobalance. This apparatus provides good accuracy

* Corresponding author. Tel.: +33 562885710; fax: +33 562885663; e-mail: Daniel.Monceau@ensiacet.fr

doi:10.1016/j.scriptamat.2007.06.018

and limits buoyancy effects by employing a symmetrical furnace arrangement. The experiment consisted of 100 cycles, with dwell times of 60 min at 1200 °C and 60 min down to 80 °C. Heating was at a constant rate of 60 °C min^{-1}, and the cooling rate was controlled at 20 °C min^{-1} down to 80 °C. Data were recorded in real time, including during heating and cooling.

A Ni–22Al–15Pt + 1 wt.% Hf specimen was cut as a thin cylinder with dimensions of 9.69 mm × 1.31 mm with an initial mass of 945.4 mg. Total gas flow rate was 1 l h^{-1}, equivalent to a linear flow rate of 1.7 cm min^{-1}. The mass change per unit surface area recorded thermogravimetrically and an enlargement showing mass change and temperature response are shown in Figures 1 and 2, respectively. The oscillations in mass change observed between cycles in Figure 2 cannot be understood in terms of simple temperature-induced buoyancy changes. Their origin is thought to be due to a combination of buoyancy and convection, arising from the fact that the symmetrical furnace arrangement was imperfect. The regulation of the two furnaces was never exactly the same, and the volumes of the sample and counterweight differed. It is to be noted that the oscillation amplitude was only 10 μg, and was perfectly reproduced every cycle.

An oxide cross-section produced by focused ion beam (FIB) milling is seen in Figure 3. Although occasional alloy protrusions almost spanned the width of the scale, it was otherwise approximately uniform. The measured average oxide thickness after 100 cycles was 3.0 ± 0.2 μm.

In order to perform a quantitative calculation on the CTGA data, the following assumptions were required:

1. No buoyancy-induced apparent mass change occurred at a fixed temperature.

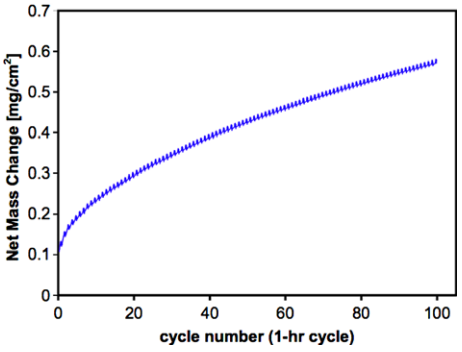

Figure 1. Cyclic oxidation kinetics as recorded by TGA.

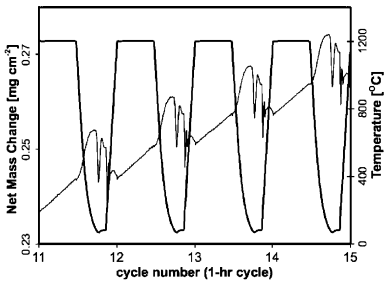

Figure 2. Net mass change (no buoyancy correction) and temperature response during cyclic oxidation.

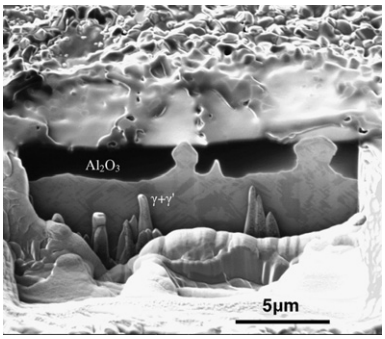

Figure 3. FIB oxide cross-section on Ni–22Al–15Pt + 1 wt.% Hf after 100 × 1 h cycle exposure at 1200 °C in dry air.

2. Oxide spallation occurred only during cooling and heating, not during reaction at high temperature. The continuous mass recording during the high temperature dwell allowed verification of this assumption.
3. Oxide formation during cooling and heating is very slow, and is negligible compared with oxidation during the high temperature dwell. This assumption can also be checked for cycles without spalling events, except during initial heating.
4. All oxides formed externally, with no internal precipitation.
5. To convert measured mass gain into an oxide scale thickness, the oxide scale is assumed to be compact and free of pores, occlusions and protrusions.
6. Materials lost by spallation are assumed to be oxide only, with no metal inclusions.
7. The oxide composition is assumed not to change throughout reaction, i.e. the metal to oxygen mass ratio in the oxide is constant.

The calculation method now described is based on the technique described by Monceau and Poquillon [10]. NMC is defined as the net mass change at the end of cycle n. The mass gain due to oxidation (ΔM_n) during a high temperature dwell can be calculated easily as

$$\Delta M_n = M_n^{\mathrm{e}} - M_n^{\mathrm{b}} \tag{1}$$

where M_n^{b} is the initial mass for cycle n at high temperature and M_n^{e} is the final mass for cycle n at high temperature. Thus, GMG_n can be defined as the cumulative mass gain of all high temperature dwells up to cycle n, and includes the mass of any oxide spalled in previous cycles:

$$\mathrm{GMG}_n = \sum_{j=1}^{n} \Delta M_j \tag{2}$$

This equation ignores the mass gain due to oxidation during initial heating. The mass of adherent oxide scale (AOX_n) per unit area of sample surface can be calculated as:

$$\mathrm{AOX}_n = \mathrm{AOX}_{n-1} + \frac{\Delta M_n}{r} - \{M_{n-1}^{\mathrm{e}} - M_n^{\mathrm{b}}\} \tag{3}$$

where r is the ratio of oxygen molar mass (M_{o}) to oxide molar mass (M_{ox}). The term in braces in Eq. (3) represents mass loss during cooling and/or heating, due to

oxide spallation. Finally, the average oxide thickness at cycle $n(e_n)$ can be calculated as

$$e_n = \frac{\mathrm{AOX}_n}{\rho} \tag{4}$$

with ρ the oxide density. This determination of average oxide thickness is useful for comparing the calculated oxide thickness with the directly measured quantity. Metal consumption can also be calculated by assuming that the scale is composed of a certain oxide [10].

Since the average adherent oxide thickness is known for each cycle, the k_p value for cycle n can be calculated by assuming that oxide formation obeys the parabolic rate law:

$$k_{p_n} = 2(\Delta m/A)\frac{\mathrm{d}(\Delta m/A)}{\mathrm{d}t} = 2r\mathrm{AOX}_n\frac{\mathrm{d}r\mathrm{AOX}_n}{\mathrm{d}t}$$
$$\approx 2r\mathrm{AOX}_n\frac{M_n^{\mathrm{e}} - M_n^{\mathrm{b}}}{\Delta t} \tag{5}$$

with $(\Delta m/A)$ the mass change per unit surface area. The percentage of oxide scale which spalled at cycle n, P_n, can be calculated simply by using:

$$P_n = 100\frac{M_n^{\mathrm{e}} - M_{n+1}^{\mathrm{b}}}{\mathrm{AOX}_n} \tag{6}$$

The assumption that oxide formation during heating and cooling is very slow and can be neglected is now considered. The high temperature dwell was 60 min and the heating time only 17 min. If the linear temperature rise is approximated as a series of several isothermal sections, the total net mass gain during heating can be calculated with isothermal k_p values at different temperatures calculated from the Arrhenius equation:

$$k_p = k_0\exp(-Q/RT) \tag{7}$$

where Q is the activation energy for Al_2O_3 growth (between 231 and 382 kJ mol^{-1} for alumina growth on Ni–50Al [14]). However, no low temperature rates are available for the test alloy, and k_0 is therefore unknown. Moreover, transitional alumina phases are expected to form at intermediate temperatures, and the calculation becomes impossible. Instead, the assumption of negligible oxidation during heating will be tested by comparing the scale thickness calculated on this basis with the directly measured value.

If oxide formation during heating and cooling is negligible, then no buoyancy correction is necessary, because only the mass recorded at high temperature is used for the analysis [10]. Since most of the oxide consisted of alumina, the $r = \frac{M_o}{M_{ox}}$ ratio and the density of the oxide scale were taken as those of pure α-Al_2O_3, for which $\rho = 4.05$ g cm^{-3} [15]. The mass of adherent oxide (AOX) and of the corresponding oxide thickness (e) were calculated from CGTA data using Eqs. (3) and (4). Oxide thickness values calculated in this way are shown in Figure 4, as a continuous line covering the first hundred cycles.

The actual average oxide thickness measured by FIB after 100 cycles was 3.0 ± 0.2 μm, which is slightly thicker than is calculated from CGTA data, but probably within experimental error. Thus, the model developed for predicting the average oxide thickness is accurate enough for this alloy in the short-term.

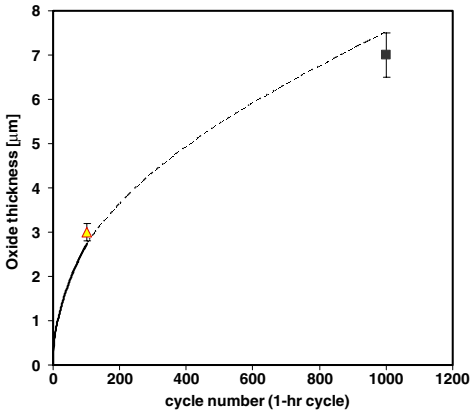

Figure 4. Oxide thickness increase. The continuous line was calculated from CTGA measurements; the dotted line extrapolated from those measurements; △ measured after CTGA experiment; ■ measured after conventional cyclic oxidation [13].

Values of P_n and k_{p_n} calculated from CGTA measurements are shown in Figure 5. A negative value of P_n corresponds to a small amount of oxide formation during heating between cycles. The neglect of this effect causes the initial mass of cycle $n+1$ to be higher than the final mass of cycle n. The k_p value for each cycle did not change much after cycle 7 from an average value of 7.5×10^{-7} mg^2 cm^{-4} s^{-1}, meaning that the oxide constitution did not change from this point. The proportion of spalled oxide P_n varied in a small range of up to 0.2% in the first 30 cycles, and was less than 0.1% between 30 and 100 cycles, showing that spallation resistance was excellent.

The utility of short-term CTGA data in predicting long-term results was tested. Conventional, discontinuous thermal cycling of the alloy was carried out for 1000×1 h cycles at 1200 °C in a controlled atmosphere of flowing dry air [13]. The average oxide thickness after 1000 cycles was measured as 7.0 ± 0.5 μm. The 100 h CTGA-derived curve in Figure 4 was extrapolated using the fixed values $P = 0.06$ % and $k_p = 7.5 \times 10^{-7}$ mg^2 cm^{-4} s^{-1}. As seen in the figure, the extrapolated curve agrees within experimental error with direct measurement. It is therefore concluded that P and k_p had reached steady-state values.

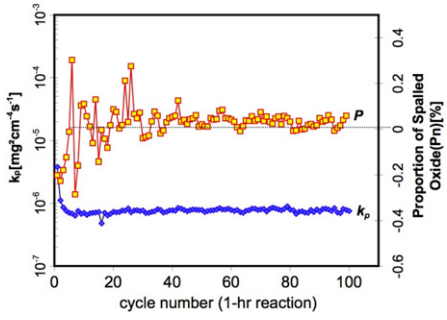

Figure 5. Instantaneous values of P_n and k_{p_n} during cyclic oxidation of NiAlPtHf.

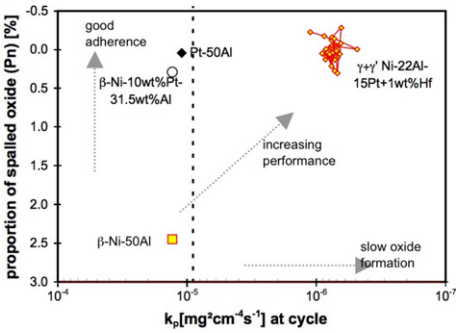

Figure 6. Performance map for cyclic oxidation at 1200 °C. Data for undoped β-Ni–50Al, Ni–10 wt.% Pt–31.5 wt.% Al and Pt–50Al were obtained from Ref. [17] after fitting to the P–k_p model [7]. The dashed line shows k_p for α-Al_2O_3 on β-NiAl [14].

The P–k_p map introduced in Ref. [7] and presented in Figure 6 can be used to compare the performance of different materials under thermal cyclic conditions [7,8,11,16]. This map allows comparison of systems with widely differing alloy-scale adherence and oxidation rates. Clearly, the best performance is achieved when the oxide–metal system has good adherence (low P_n) and a slow growing oxide (low k_{p_n}). The current results for Ni–22Al–15Pt + 1 wt.% Hf reflect the findings of Figure 5: after some initial changes, P_n and k_p became rather constant. Previous findings for different alloys oxidized at the same temperature and in a laboratory atmosphere [17] have been analysed in Ref. [7]. The Ni–22Al–15Pt + 1 wt.% Hf has a slower oxidation rate than undoped β-Ni–50Al, Ni–31.5Al–10Pt and Pt–50Al. It has a much better spallation resistance than undoped β-Ni–50Al. Its spallation resistance is similar to that of β-NiAl modified with 10 wt.% of platinum and Pt–50Al, but with a much lower k_p. The significance of the relatively small differences in P and k_p between Pt–50Al and Ni–22Al–15Pt + 1 wt.% Hf can be appreciated from a calculation of the time at which the NMC becomes negative. This can be evaluated using the P–k_p model to extrapolate experimental data. For the Pt–50Al alloy, NMC becomes negative after 3000 cycles, whereas for Ni–22Al–15Pt + 1 wt.% Hf this does not occur until 5100 cycles.

It is well known that β-phase Ni–Al binary alloys with their high aluminium content are pure alumina formers, while the two-phase γ + γ′ alloy tends to form more nickel-rich transient oxides [18]. The addition of Pt at levels as low as 15 at.% clearly promotes alumina formation on the γ + γ′ alloy and also significantly improves its spallation resistance compared with the β-phase alloy. In addition, doping with 1 wt.% Hf reduces the alumina growth rate to values even lower than that measured [14] for α-Al_2O_3 growth on β-Ni–50Al under isothermal conditions.

Several explanations have been given for the positive effect of Pt on the cyclic oxidation of alumina formers. Pt additions may promote alumina by modifying metal transport within the alloy [19]. Pt also caused the formation of protrusions, which could improve the oxide adherence by a mechanical keying mechanism [20]. It also prevents internal oxidation by reducing the oxygen permeability within the alloy [19]. The alloy sulfur content is also correlated with spallation [21]. Hafnium is a reactive element and may chemically bind sulfur in the alloy as a separate phase or as a segregant. It is also thought to slow oxide growth by suppressing cation transport across the alumina scale [21–23]. Thus, oxide formation depends only on oxygen transport across the scale and takes place at the oxide–metal interface.

The P–k_p map shows the cyclic oxidation performance of Ni–22Al–15Pt + 1 wt.% Hf, using kinetic data measured by cyclic thermogravimetry analysis (CTGA). The studied alloy forms an oxide scale with excellent adherence and very low growth rate, and its promise as a coating material candidate [24] is confirmed. Indeed, at 1200 °C and in a dry air environment, the addition of 15 at.% Pt and 1 wt.% Hf to Ni–22Al provided better performance in a cyclic oxidation test than that of undoped β-Ni–50Al, Ni–10 wt.% Pt–31.5 wt.% Al and Pt–50Al. Nevertheless, it should be noted that this test was short (100 h). Longer tests would be necessary to check if this excellent behaviour can be retained.

[1] J.R. Nicholls, M.J. Bennet, in: M. Schütze, W.J. Quadakkers (Eds.), Cyclic Oxidation of High Temperature Materials (EFC 27), Maney, London, 1999, p. 437.
[2] H.J. Grabke, D.B. Meadowcroft (Eds.), Guidelines for Methods of Testing and Research in High Temperature Corrosion (EFC 14), Maney, London, 1995, p. 234.
[3] J.R. Nicholls, R. Newton, M.J. Bennet, H.E. Evans, H. Al-Badairy, G.J. Tatlock, D. Naumenko, W.J. Quadakkers, G. Strehl, G. Borchardt, in: M. Schütze, W.J. Quadakkers, J.R. Nicholls (Eds.), Lifetime Modelling of High Temperature Corrosion Processes (EFC 34), Maney, London, 2001, p. 15.
[4] B.A. Pint, P.F. Tortorelli, I.G. Wright, in: M. Schütze, W.J. Quadakkers (Eds.), Cyclic Oxidation of High Temperature Materials (EFC 27), Maney, London, 1999, p. 111.
[5] J.L. Smialek, G.N. Morscher, Mat. Sci. Eng. 332 (2002) 11.
[6] J.L. Smialek, Met. Trans. 9A (1978) 309.
[7] D. Poquillon, D. Monceau, Oxid. Met. 59 (2003) 409.
[8] N. Vialas, D. Monceau, B. Pieraggi, Mat. Sci. Forum 461–464 (2004) 747.
[9] J.C. Pivin, D. Delaunay, C. Roques-Carmes, A.M. Huntz, P. Lacombe, Corros. Sci. 20 (3) (1980) 351.
[10] D. Monceau, D. Poquillon, Oxid. Met. 61 (2004) 143.
[11] A. Raffaitin, D. Monceau, E. Andrieu, F. Crabos, Acta Mater. 54 (2006) 4473.
[12] V. Deodeshmukh, N. Mu, B. Li, B. Gleeson, Surf. Coat. Technol. 201 (2006) 3836.
[13] R. Kartono, D.J. Young, Mater. Corros., in press.
[14] M.W. Brumm, H.J. Grabke, Corros. Sci. 33 (1992) 1677.
[15] NBSCAA, vol. 9, 1960, p.3.
[16] J.L. Smialek, Acta Mater. 52 (2004) 2111.
[17] B.A. Pint, I.G. Wright, W. Lee, Y. Zhang, K. Prußner, K. Alexander, Thermal barrier coating workshop, NASA Technical Report 19980214845, 1997, pp. 109–125.
[18] F.S. Pettit, Trans. AIME 239 (1967) 1296.
[19] B. Gleeson, W. Wang, S. Hayashi, D. Sordelet, Mat. Sci. For. 461–464 (2004) 213.
[20] E.J. Felten, F.S. Pettit, Oxid. Met. 10 (1976) 189.
[21] J.G. Smeggil, A.W. Funkenbusch, N.S. Bornstein. Met. Trans. 17A (1986) 923.
[22] B.A. Pint, J.R. Martin, L.W. Hobbs, Oxid. Met. 39 (1993) 167.
[23] B.A. Pint, Oxid. Met. 45 (1996) 1.
[24] B.Gleeson, D.J. Sordelet and W.Wany, US Patent Application No. 2004 0229075, 2004.